J. Membrane Biol. 206, 61–72 (2005)
DOI: 10.1007/s00232-005-0774-1

The Journal of
Membrane
Biology

Electrogenic H^+ Transport and pH Gradients Generated by a V-H^+-ATPase in the Isolated Perfused Larval *Drosophila* Midgut

S. Shanbhag, S. Tripathi
Tata Institute of Fundamental Research, Mumbai 400 005, India

Received: 21 September 2005

Abstract. A method for microperfusion of isolated segments of the midgut epithelium of *Drosophila* larvae has been developed to characterize cellular transport pathways and membrane transporters. Stereological ultrastructural morphometry shows that this epithelium has unusually long tight junctions, with little or no lateral intercellular volume normally found in most epithelia. Amplification of the apical and basal aspects of the cells, by $\approx$ 17-fold and $\approx$ 7-fold, respectively, predicts an almost exclusively transcellular transport system for solutes. This correlates with the high lumen-negative transepithelial potential (V_t) of 38 to 45 mV and high resistance (R_t) of 800 to 1400 $\Omega \bullet cm^2$ measured by terminated cable analysis, in contrast to other microperfused epithelia like the renal proximal tubule. Several blockers (amiloride 10^{-4} M, ouabain 10^{-4} M, bumetanide 10^{-4} M), K^+-free solutions, or organic solutes such as D-glucose 10 mM or DL-alanine 0.5 mM failed to affect V_t or R_t. Bafilomycin-A_1 (3 to 5 μM) decreased V_t by $\approx$ 40% and short-circuit current (I_{sc}) by $\approx$ 50%, and decreased intracellular pH when applied from the basal side only, consistent with an inhibition of an electrogenic V-H^+-ATPase located in the basal membrane. Gradients of H^+ were detected by pH microelectrodes close to the basal aspect of the cells or within the basal extracellular labyrinth. The apical membrane is more conductive than the basal membrane, facilitating secretion of base (presumably HCO_3^-), driven by the basal V-H^+-ATPase.

Correspondence to: S.Tripathi; email: tripathi@tifr.res.in

Abbreviations BEL, basal extracellular labyrinth; DMSO, dimethylsulfoxide; HEPES, N-2-hydroxyethylpiperazine-N'-2-ethaesulfonic acid; I_{sc}, short-circuit current; LIS, lateral intracellular space; R_t, transepithelial resistance; V_a, apical cell membrane potential; V_b, basal cell membrane potential; V-H^+-ATPase, vacuolar-proton-adenosinetriphosphatase; V_t, transepithelial potential, perfusion end; V_c, transepithelial potential, collection end.

Key words: Bafilomycin-A_1 — Ultrastructural morphometry — Cable analysis — Ion-selective microelectrodes — Microperfusion

Introduction

The principle function of the insect midgut is to digest and absorb nutrients and is the first line of defence against ingested pathogens and toxins. Physiological studies of epithelial transport in many insect species, including larval fruitfly, have neglected the midgut, despite the fact that it is by far the largest epithelial organ system and probably a major site of uptake of ingested nutrients, solutes and water. Modulation of the pH within the gut lumen is an essential prerequisite for enzymatic action, and the pH along the digestive tract varies markedly among orders of insects, presumably as an adaptation to diet (Dow, 1984; Klein et al., 1996; Terra et al., 1996; Boudko et al., 2001a). High pH values have been recorded in anterior midgut of several mosquito larvae, including *Aedes aegypti* (Dadd, 1975), as well as in some lepidopteran larvae with high tannin diet (Berenbaum, 1980). The alkaline environment of the anterior midgut lumen enhances dissociation of tannin-protein complexes and subsequent digestion and absorption of tannin-free protein at the near neutral pH of the posterior midgut (Martin & Martin, 1984; Schultz & Lechowicz, 1986; see Harrison, 2001). This pattern of nutrient processing leads to sizeable gradients of pH and ionic concentration along the length of the gut. Successive zones of acid secretion and downstream neutralization were confirmed by pH-sensitive dyes and microelectrode measurements in house flies and mosquitoes (Greenberg, 1968; Boudko et al., 2001b). Thus, while the middle midgut is alkaline (pH $>$ 10) in some insects (*see* Dow, 1986; Klein et al., 1996; Zhuang et al., 1999), it is acidic (pH $<$ 3) in many

dipterans (Dubreuil et al., 1998; 2001), as in the gastric epithelium of vertebrates. The generation of large pH gradients over short distances in the absence of morphological barriers is possibly the result of region-specific ion transport systems energized by a plasma membrane V-H$^+$-ATPase (Dow, 1992; Filippova et al., 1998; Zhuang et al., 1999; Boudko et al., 2001b; Wagner et al., 2004), but a comprehensive description of solute and water transport is not available. Moreover, little is known of the ultrastructure and electrophysiology of *Drosophila* midgut regions in which a monolayer of a small number of epithelial cells make them attractive preparations for transport studies. Clearly, not much data can be gleaned without independent access to both sides of the epithelia.

We have addressed the technical difficulties of studying this epithelium by drawing upon the experience with other epithelia where such combined studies were possible (Tripathi, Boulpaep & Maunsbach, 1987). We report the first microperfusion electrophysiology and ultrastructural stereology of the *Drosophila* midgut epithelium. Surprisingly, there is no lateral intercellular space and an extensive extracellular basal labyrinth (BEL) is the main compartment for transport coupling. Electrophysiology, with full access to both surfaces of the epithelial cells, shows that the *Drosophila* midgut is a tight epithelium and verifies the asymmetry of the apical and basal membrane areas predicted by stereological ultrastructural measurements reported here. The basis of luminal alkalinization is shown to be based on net transepithelial H^+ extrusion to the hemolymph by an electrogenic V-H$^+$-ATPase located in the basal membrane. A preliminary account of the results has appeared in abstract form (Shanbhag & Tripathi, 2005).

Materials and Methods

Fly Stocks and Segmental Luminal pH

Actively feeding third instar larvae of *Drosophila melanogaster* Canton S (CS) strain were reared in a cornmeal-sugar-agar medium supplemented with dry yeast and kept at room temperature (≈ 22°C) under a 22 –24 hour day/night cycle. Midguts from actively feeding, third instar larvae were dissected out carefully in *Drosophila* Ringer's solution (Ashburner, 1989). The midgut was removed from the dissection Ringer, pH 7.2, and placed on a piece of universal pH indicator paper (pH range 1–10). By pressing gently, the luminal content of the midgut was released and the change in coloration of the pH paper was scanned. Colors generated by pH standards of 1 to 11 on the same pH paper were also scanned for calibration.

Solutions and Microperfusion

The composition and osmolarity of the perfusion and superfusion solutions and fixatives are given in Table 1. The pH of solutions was adjusted to 7.2 while stirring and bubbling with the 95% O_2 – 5% CO_2 gas mixture used during the experiment. All chemicals and reagents were obtained from Sigma-Aldrich-Fluka. Bafilomycin-A_1 was dissolved in 1% dimethyl-sulfoxide (DMSO), diluted with-standard Ringer (*Solution a*) to a final concentration of 1 to 5 μM and stored at −20 °C until use. DMSO applied without Bafilomycin-A_1 at concentrations between 0.1 to 1% had no effect on transepithelial potentials. Perfusate concentrations of DMSO were $< 0.1\%$.

Middle or posterior midgut segments (1–2 mm long) were cannulated (initially at one end and subsequently at both ends) and perfused in vitro using methods described previously (Tripathi et al., 1987) for optimal control of hydrodynamic conditions of axial flow and transepithelial pressure. The microperfusion apparatus and microforge equipment were built in the laboratory. Spontaneous contractions of the gut became quiescent after initiation of perfusion without the addition of any smooth muscle inhibitors. A patent lumen (diameter 140 to 200 μm) and axial flow of ≈200 nl / min, was ensured at all times. Solution composition along the lumen was thus controlled and invariant and perfusion-end hydrostatic pressure was < 3 cm H_2O. The bath (≈200 μl) was also exchanged rapidly (> 3 ml / min) by gravity perfusion. The same perfusion and collection pipette assemblies were used for all morphometric experiments. All solutions were delivered to pipettes or chamber by gravity through PVC tubing. Experiments were done at room temperature (21–23°C).

Ultrastructural Morphometry

Experimental Groups

Segments of isolated posterior midgut, single-end cannulated and perfused in vitro, were treated in four groups: *A*) control, HEPES-Ringer (Table 1, *Solution b*) in lumen and bath; *B*) Na^+-free Ringer (*Solution d*) in lumen and HEPES-Ringer in bath; *C*) HEPES-Ringer (*Solution b*) in lumen and Na^+ -free Ringer (*Solution d*) in bath; *D*) Na^+ -free Ringer (*Solution d*) in lumen and bath.

Fixation of Gut Segments in Vitro

Posterior midgut segments were dissected in HEPES-Ringer solution (Table 1, *Solution b*). After a control period of perfusion with HEPES-Ringer for assessing viability and controlling hydrodynamic parameters, the gut was perfused-superfused with the solution pairs grouped above. Once the transepithelial potentials had reached a steady state (5–7 min), the gut was fixed with *Solution f* (Table 1) from the bath.

For light and electron microscope observations, small pieces of posterior midgut were fixed for 2–4 h in 2.5% solution of glutaraldehyde buffered to pH 7.4 with 0.08 M cacodylate buffer at room temperature. Subsequent processing was as described in Shanbhag et al. (1992). The sections were then stained with uranyl acetate and lead citrate and examined in a JEOL JEM 100S electron microscope.

Morphometric analysis was carried out on complete gut cross-sections oriented perpendicular to the axis of the dissected posterior midgut segment. Overlapping electron micrographs were taken at a magnification of ×3,500, enlarged to ×7,000 and assembled in montages. The smallest outer diameter of the midgut was determined on the semithin section. The luminal diameter was determined along the same radial line as was the outer diameter. Cell height (not including microvilli) was calculated as difference between the outer and luminal diameters. Volume densities, volumes, and surfaces of midgut structures or extracellular spaces were computed from point and intersection counting as previously described in detail (Maunsbach & Boulpaep, 1984).

Table 1. Composition of Ringer solutions and fixative

Component	Solutions					
	a	*b*	*c*	*d*	*e*	*f*
NaCl	130.0	130.0			135.0	
$NaHCO_3$	10.0		10.0		10.0	
NaH_2PO_4	0.5	0.5	0.5		0.5	
Na_2HPO_4	0.1	0.1	0.1		0.1	
$CaCl_2$	1.8	1.8		1.8	1.8	
$MgCl_2$	1.0	1.0		1.0	1.0	
DL-alanine	0.5	0.5	0.5	0.5	0.5	
D-Glucose	10.0	10.0	10.0	10.0	10.0	
KC1	5.0	5.0		5.0		
KH_2PO_4				0.5		
K_2HPO_4				0.1		
HEPES		10.0		10.0		
N-methyl D-glucamine				130.0		
D-Gluconic acid Na-salt			130.0			
D-Gluconic acid K-salt			5.0			
D Gluconic acid Hemi Mg-salt			1.0			
Ca-D-gluconate			1.8			
Cacodylate$^-$						76.26
Cacodylic acid						3.74
Glutaraldehyde, %						2.5
Osmolarity, mosM	282	279	273	281	280	506
Resistivity, Ω • cm	93	96	187	137	96	

Solution a, substrate Ringer; *Solution b*, HEPES Ringer; *Solution c*, Cl^--free Ringer; *Solution d*, Na^+-free Ringer; *Solution e*, K^+-free Ringer; *Solution f*, standard fixative. Concentrations are in mM except for glutaraldehyde. The pH of perfusion-superfusion solutions were titrated to 7.2 with either KOH or HC1. Solutions *a, c* and *d* were bubbled with a 5% CO_2 and 95% O_2 gas mixture and solutions *b* and *d* with 100% O_2 gas. pK of cacodylic acid is 6.19. Trypan blue dye was added to solution in lumen to exclude cell damage at the beginning of each experiment, but was not present during fixation or physiological recording.

Electrophysiology, Data Acquisition and Analysis

Electrophysiological Measurements

Transepithelial potential was measured through the perfusion (V_t) and collection (V_c) pipettes and Ringer-agar bridges connected to electrometers. Following cannulation of the perfusion end, it was essential to cannulate the distal (collection) end within 3 or 4 minutes, as a contracted gut is difficult or impossible to open without applying high pressures with attendant damage. The preparation was allowed to stabilize for at least twenty minutes over which period the electrical seal with the holding pipettes was established and V_t and V_c reached steady state.

Transepithelial resistance R_t ($\Omega \bullet cm^2$) was measured by injection of current pulses of 100 nA through the bridge-balance electrometer probe at the perfusion end and measuring the attenuation of the potential step at the collection end (Tripathi & Boulpaep, 1988). The luminal epithelial surface is treated as a cylindrical cable terminated at perfusion and collection ends, using the relationships:

$$L/\lambda = \cosh^{-1}(\Delta V_t/\Delta V_c) \quad (1)$$

$$R_t = 2(\pi\lambda^3 R_{in} R_S \tanh L/\lambda)^{1/2} \quad (2)$$

where L (cm) is distance between the tips of the perfusion and collection pipettes in the lumen, λ (cm) is the length constant of the midgut epithelium, ΔV_t(mV) is the displacement in potential at perfusion end, ΔV_c (mV) is the attenuated potential at the collection end, R_{in} (Ω) the input resistance of the midgut segment, and R_s ($\Omega \bullet$ cm) the volume resistivity of the luminal perfusate (*see* Table 1).

Cell membrane potentials were measured from the basal side (V_b) using conventional microelectrodes (resistances of 30–60 MΩ and tip potentials < 2 mV) made from 1-mm-OD borosilicate fiber capillaries (Omega Dot) obtained from Frederick Haer (Bowdoinham, ME) and filled with 0.5 M KCl; these electrodes were pulled on a horizontal puller (Narishige, Tokyo, Japan, model PN-3). Apical membrane potential V_a was calculated as the difference between transepithelial (V_t) and basal (V_b) potentials. V_t, V_c and V_b were measured with electrometers (WPI, Sarasota, FL, models M-707 or 705).

Liquid-ion-exchanger pH-selective microelectrodes were fabricated on a Sutter P-97 puller (Sutter, Novato, CA) from aluminosilicate glass (Sutter, cat. no. A150-100-10) and silanized as described by Tripathi, Morgunov & Boulpaep, (1985) in a glass oven at 150°C. Hydrogen ionophore I cocktail A (Fluka, cat. no. 95291) was used as the sensor. The electrodes were back-filled with 0.1 M HCl and fitted with Ag/AgCl half-cells. Tip diameters were < 1 μm and time constants for response to solution changes were 10–20 s. The microelectrodes were calibrated in pH 4.01 and pH 7.01 buffers and had slopes between 55–62 mV / pH unit ($n = 33$). Electrode resistances were ≈ 10 GΩ and model FD 223 or Duo 773 (WPI) electrometers were used for pH microelectrodes. Simultaneous impalements of adjacent or neighboring cells yield identical V_b values, indicating that the cells are electrically coupled. Therefore, intracellular pH (pH_i) was determined from the difference between the potentials of the pH-selective and membrane potential microelectrodes simultaneously inserted two or three cells apart. When precision positioning of microelectrodes was required, a piezo-stepper (EXFO inchworm, model 8200, Montreal, Canada) was used. All electrode signals were filtered at 30 Hz (low pass 4-pole Bessel) and acquired on a computer using a National

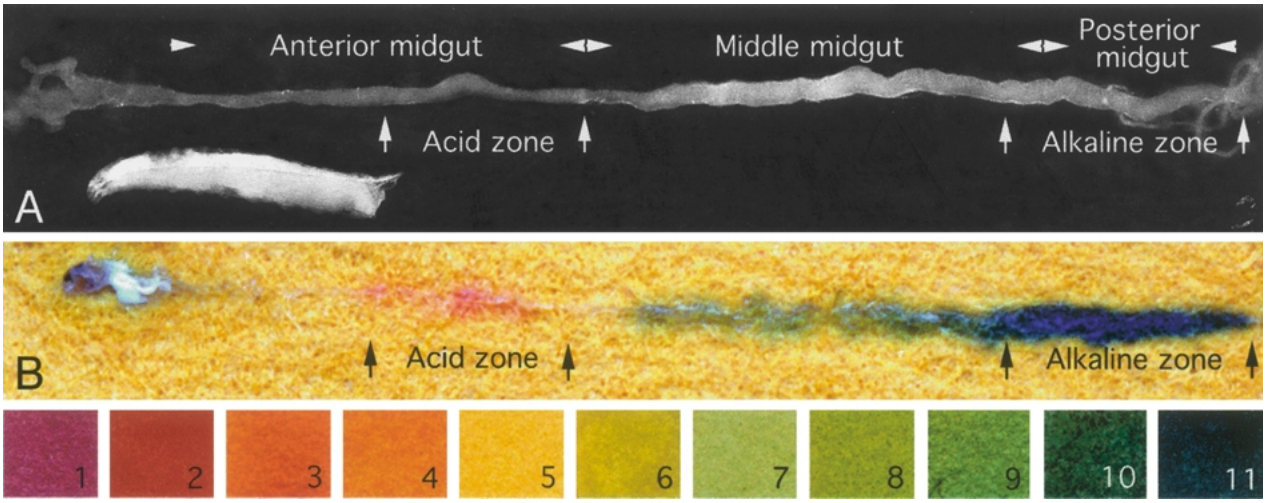

Fig. 1. (*A*) An active third-instar intact *Drosophila* larva (≈3mm long) is shown below a dissected larval midgut, from its proventricular end on the left to its caudal junction with the Malpighian tubule on the right. (*B*) Luminal content pH detected by pH-paper shows, from left to right, a distinct acid-secreting zone, followed by a neutral and lastly an alkaline segment. Lower numbered panels denote colors generated by pH standards of 1 to 11. Data presented in this study are from perfusion of middle and posterior midgut segments.

Instruments PCI-6110 data acquisition card and a BNC-2110 breakout box. A custom software using Labview 6i version 6.0.2 on Windows 2000 was used to display and record data directly on disc.

Statistical Analysis

All data are expressed as means ± SEM. Significance of the differences in morphometric data between groups of midgut cells was evaluated by an unpaired two-tailed Student's *t*- test. For each group, no more than one posterior midgut segment was derived from each animal. Viability was ascertained by exclusion of trypan blue dye added to Solution a in the lumen; any preparation with staining of even a single cell was rejected. Data included in this study were from preparations with a minimum V_t of 20 mV.

Results

Segmentation of Midgut

Figure 1*A* shows the gut of a larva dissected out. The luminal contents of the midgut were released gently onto pH indicator paper. From the reaction of the luminal contents with the pH paper, distinct variation of luminal pH along the length of the midgut epithelium was measured (Fig. 1B). The anterior midgut segment was neutral and was followed by an acid zone. The diameter of the midgut immediately following the acid zone appeared to be of the appropriate size for reliable microperfusion. This was an alkaline segment with the pH increasing towards the caudal end. Results were collated from three independent experiments. As the first and second halves (middle midgut and posterior midgut) were different, each was perfused separately and results are presented separately unless indicated otherwise.

Ultrastructural Morphometry

As the *Drosophila* midgut epithelium has not been studied from a physiological viewpoint, it was essential to define the epithelial architecture and to further localize transport systems to develop models for solute and water transport. A thin mesenchymal membrane isolates the circular and longitudinal muscles and the tracheal tubes from the larval hemolymph (Fig. 2). The peritrophic membrane, the epithelial layer, basement membrane and the mesenchymal membrane appear to be the contiguous diffusion barriers between the lumen of the gut and the hemolymph (Fig. 2B). The fine structure of cells in the perfused midgut is similar to that of unperfused midgut except for a marginal reduction in cell height and the sweeping away of the peritrophic membrane (Figs. 2 and 3B).

Five or six cells span the circumference of the midgut epithelium (Fig. 2*A* and Table 2). They are flat cells, ≈ 100 μm wide and ≈ 12 μm high (including microvilli). The apical region, which forms the border to the tubule lumen, has a brush border with numerous microvilli (Figs. 2*B* and 3*B*). These cells possess elaborate cytoarchitecture with abundant mitochondria (Figs. 2*B* and 3*A*). The cell population is for the most part homogeneous; about 10% of these cells are less electron-dense, granulated, with fewer mitochondria, and shorter microvilli and have less basal infolding. Most cells have extensive membrane folds of the basal plasma membrane that penetrate almost halfway into the cells (Fig. 3*A, C*). Several mitochondria are also closely associated with these basal membrane foldings. The lateral cell borders are connected by septate junctions and desmosomes

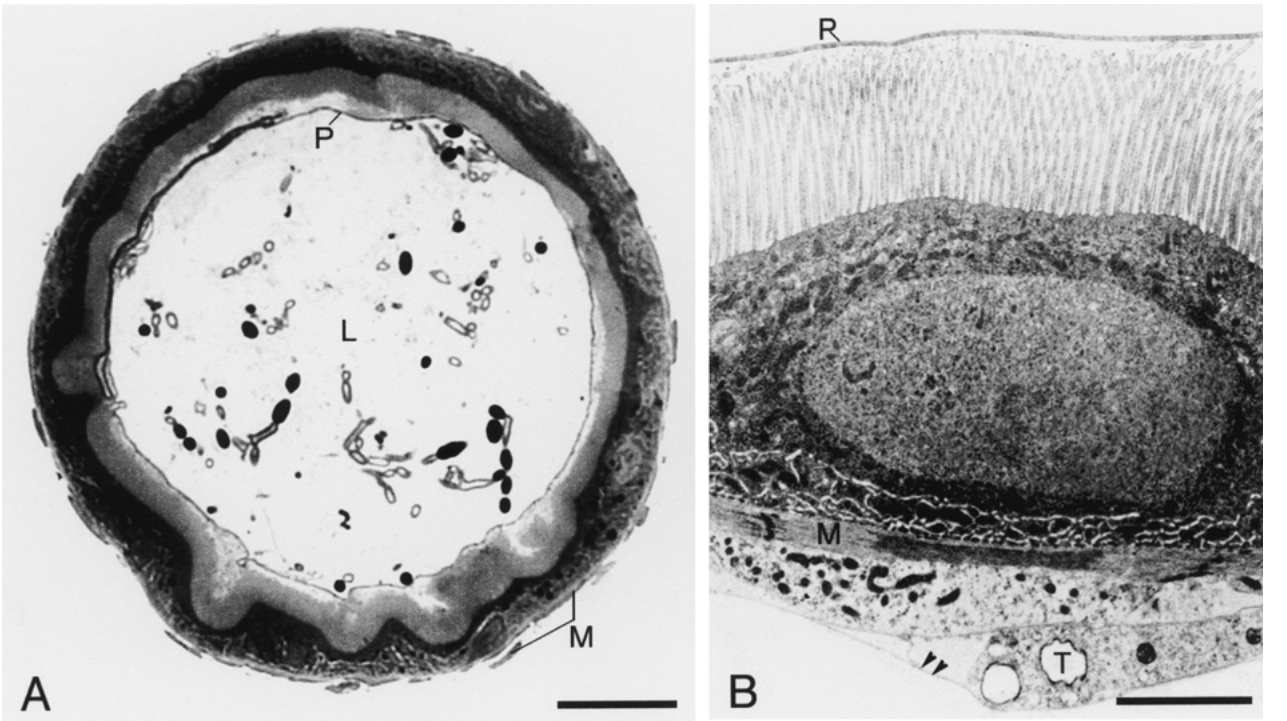

Fig. 2. (*A*) The midgut epithelium in cross-section. Scale Bar: 40 μm *L*: lumen; *P*: peritrophic membrane normally present in vivo. 5–6 cells span the circumference in a single layer, (*B*) The wall of an unperfused midgut is shown with intact peritrophic membrane covering the microvilli of the luminal epithelial surface. This peritrophic membrane is swept away with the commencement of perfusion. The basal membrane is separated from the hemolymph by muscles (*M*) and trachea (*T*). Double-arrowheads indicate the outermost diffusion barrier. Scale Bar: 2 μm

(Fig. 3*A*). The junction begins apically at the luminal epithelial surface of the midgut and proceeds basally almost halfway down the cell. The lateral intracellular space (LIS) between the two adjacent epithelial cells is negligible. Figure 3 is a longitudinal section of two adjacent epithelial cells, depicting the types of membrane specialization present. The apical and basal membrane amplification is substantial (Table 2), bounding extracellular compartments on both apical and basal aspects of the cell where solute-solvent interaction could take place. Cells are joined tightly to each other in the luminal half of their height with extremely long junctional complexes. For the purpose of stereological analysis we define the basal extracellular labyrinth (BEL) as the annular extracellular volume between the radially outermost terminus of intercellular junctions (Fig. 3*A*, arrow) and the basement membrane. Cell volume (inclusive of microvillar volume) was calculated as the gut wall volume less the extracellular volume. BEL volume density, expressed as μm^3 / μm^3 of midgut wall, was calculated from the BEL volume and the gut wall volume.

To test the possible effects of inhibition of transport on dimensions of membrane areas or compartmental volumes, midgut segments were perfused in the lumen with Na^+-free Ringer (Solution d) and fixed (Solution f). No significant effects on the gut outer and luminal diameter, luminal volume, cell height or basement membrane surface area were noticed (Table 2, column 3). However, a significant reduction in BEL volume was observed. Perfusion with Na^+-free Ringer in the bath only reduces the volume of the BEL to negligible levels and large empty vacuoles appear in the cytoplasm (Table 2, column 4). Bilateral perfusion with Na^+-free Ringer reduces cell volumes and microvillar height; *no BEL volume is seen*. Cells also accumulate large empty vacuoles and spaces in the cytoplasm (Table 2, column 5), correlating with the loss of plasma membrane.

Electrophysiology

Figure 4 shows measurements of transepithelial potential as recorded by the perfusion (V_t) and collection (V_c) micropipettes. Cannulation and initiation of perfusion showed a lumen-negative V_t of approximately −20 mV (−13.4 ± 0.6 mV, (n = 54), in the middle midgut and −18 ± 0.3 mV, (n = 202), for the posterior midgut, respectively). Cannulation of the collection end further increased V_t, up to −45 mV (−37.8 ± 0.8 mV and −52.2 ± 0.8 mV in the middle and the posterior midgut, respectively). Current pulses (≈ 100nA) injected into the proximal perfusion pipette through a bridge balance electrometer caused

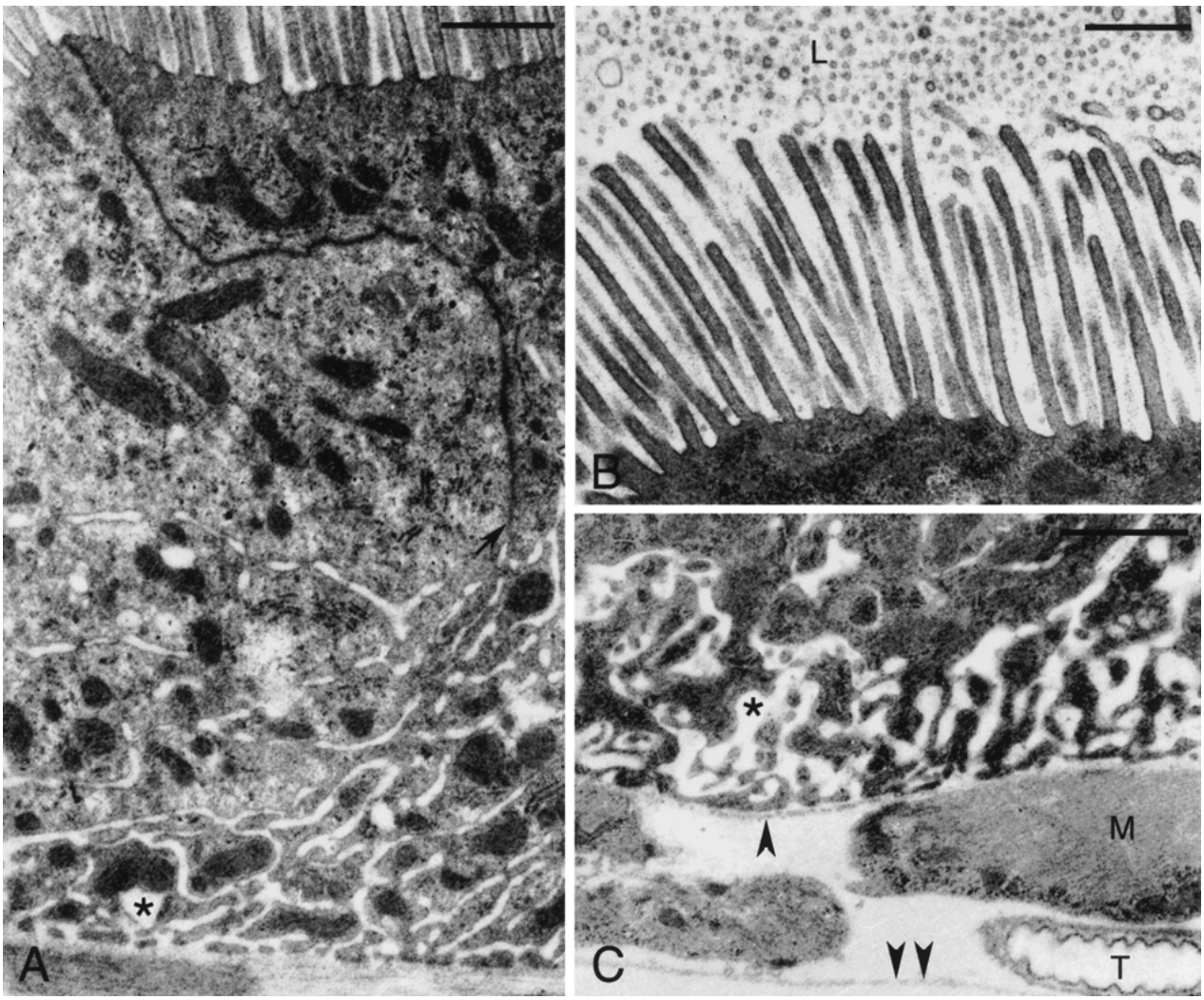

Fig. 3. (*A*) Intercellular junction of perfused midgut epithelium. The lateral membranes of adjacent cells extend from the junctional complex at the luminal epithelial surface and terminate (*arrow*) in the basal extracellular labyrinth (∗). There is no intercellular space except for an occasional small vacuole-like space in some sections. Scale Bar: 1 μm. (*B*) Brush-border of a perfused midgut shows the absence of a peritrophic membrane with a direct access of the intact microvilli to the luminal solution (*L*). Scale Bar: 1 μm. (*C*) The basal membrane encloses a significant basal extracellular labyrinth (∗) up to the basement membrane surface (*single arrowhead*) and a small path to the bulk solution via the outermost muscle layer (*M*), trachea (*T*) and the outermost surface barrier (*double arrowhead*). Scale Bar: 0.5 μm.

appropriate displacements of V_t from which transepithelial resistance (R_t) could be measured as described in Methods. Release of the collection pipette (Fig. 4, *) reduces V_t at the perfusion end. Release of the perfusion end restores all pipette potentials to zero (Fig. 4*A, C, arrows*). This suggests that the midgut epithelium is a tight epithelium with a high R_t, unlike most perfused epithelial preparations, e.g., the proximal renal tubules or gastric glands (Tripathi & Boulpaep, 1988). The middle midgut, which immediately follows the acid zone, appears to have a lower H^+ transport capacity (Fig. 1*B*). This is confirmed in Fig. 4 where lower panels (Fig. 4*C*, *D*) show that the posterior midgut develops higher transepithelial potentials than the middle midgut.

Figure 5 shows the effect of bilateral substitution of HCO_3^- with HEPES (Solution a replaced with Solution b). V_t depolarized from -33.5 ± 1.6 to -28.2 ± 1.4 mV ($n = 33$; $P < 0.001$), which correlates with depolarization of the basal membrane V_b and a much smaller depolarization of V_a. In the middle midgut R_t changes were equivocal (984 ± 57 $\Omega \bullet cm^2$ in HCO_3^- Ringer and 909 ± 57 $\Omega \bullet cm^2$ in HEPES Ringer, $n = 33$; $p \geq 0.05$). R_t in the posterior segment was unaffected by replacement of HCO_3^- with HEPES Ringer (1212 ± 103 $\Omega \bullet cm^2$ in HCO_3^- Ringer and 1141 ± 82 $\Omega \bullet cm^2$ in HEPES Ringer, $n = 15$, $p > 0.1$).

Bilateral removal of Chloride (Solution a replaced with Solution c) produced an initial large

Table 2. Quantitative ultrastructural analysis of posterior mid gut segment in *Drosophila melanogaster*

	Unperfused	Perfused, single-end cannulated			
Luminal solution: Bath solution:		Control (*b*) Control (*b*)	Na^+-free (*d*) Control (*b*)	Control (*b*) Na^+-free (*d*)	Na^+-free (*d*) Na^+-free (*d*)
Gut outer diameter, μm	180 – 200	160 – 180	160 – 180	160 – 180	160 – 180
Luminal diameter, μm	150 – 172	140 – 160	140 – 160	140 – 160	144 – 184
Cell height (excluding microvilli), μm	11.01 ± 0.36	7.80 ± 0.05	7.60 ± 0.30	7.60 ± 0.30	5.70 ± 0.30
Microvillus height, μm	3.25 ± 0.10	2.54 ± 0.12	2.33 ± 0.11	2.77 ± 0.07	1.79 ± 0.05
Microvillus number/μm^2	31.00 ± 0.18	29.80 ± 0.04	36.70 ± 0.12	23.50 ± 0.13	19.00 ± 0.06
Microvillus volume, mean, μm^3	0.042	0.033	0.030	0.036	0.023
Microvillar amplification	17.75 ± 0.80	12.79 ± 0.79	12.93 ± 0.41	11.29 ± 0.42	8.02 ± 0.34
Luminal membrane surface, mean, (excluding microvilli) 10^3 μm^2/mm length	506.00	471.43	471.43	471.43	515.43
Basement membrane surface area, mean, 10^3 μm^2/mm length	597.14	534.29	534.29	534.29	534.29
Basal extracellular labyrinth amplification	7.17 ± 0.43	6.09 ± 0.54	2.95 ± 0.24	1.13 ± 0.18	1.51 ± 0.20
Cell volume, mean, 10^6 μm^3/mm length	5.64	3.71	3.84	3.98	2.96
Basal extracellular labyrinth volume, mean, 10^6 μm^3/mm length	0.59	0.43	0.26	0.0	0.0
Vacuolar volume, 10^6 μm^3/mm length	0.04 ± 0.01	0.07 ± 0.01	0.28 ± 0.07	0.37 ± 0.06	0.34 ± 0.12

Solutions present prior to fixation are shown in parentheses. Data are reported as means from at least 10 cells or at least 10 complete tubular midgut wall sections.

hyperpolarization that settled to a lower hyperpolarized potential (Fig. 6 *A, B*). V_t was restored partially with control Ringer. R_t increased from 1100 ± 276 Ω • cm^2 to 2552 ± 610 Ω • cm^2 ($n = 8$, $P < 0.004$) and from 819 ± 82 Ω • cm^2 to 2592 ± 372 Ω • cm^2 ($n = 8$, $p < 0.001$) in the middle and posterior midgut, respectively. Calculated short-circuit current (I_{sc}), in the middle midgut decreased from 41 ± 7.2 μA • cm^{-2} to 18 ± 4.5 μA • cm^{-2} ($n = 8$; $p < 0.004$); likewise, I_{sc} in the posterior midgut segment decreased from 63 ± 5 μA • cm^{-2} to 23 ± 2.8 μA • cm^{-2} ($n = 8$; $p < 0.001$) after bilateral Cl^- removal.

Bilateral removal of Na^+ (Solution b replaced with Solution d) depolarized V_t from −35 mV to −26 mV and −60 mV to −36 mV in the middle and posterior midgut, respectively, after an initial hyperpolarization (Fig. 6 *C, D*). Restoration of control Ringer restored V_t to control values. Bilateral Na^+-free microperfusion significantly increased R_t from 881 ± 103 Ω • cm^2 to 1490 ± 140 Ω • cm^2 ($n = 9$, $p < 0.001$) in the middle midgut and from 1146 ± 162 Ω • cm^2 to 2169 ± 272 Ω • cm^2 ($n = 7$, $p < 0.006$) in the posterior midgut segments. Calculated short-circuit current (I_{sc}), in middle midgut decreased from 25 ± 2.6 μA • cm^{-2} to 16 ± 1.8 μA • cm^{-2} ($n = 9$; $p < 0.05$); likewise, I_{sc} in the posterior midgut segment decreased from 40 ± 5 μA • cm^{-2} to 26 ± 3.7 μA • cm^{-2} ($n = 7$; $p < 0.05$) after bilateral Na^+ removal.

Bilateral removal of K^+ (Solution a replaced with Solution e) or substrates (10 mM glucose and 0.5 mM DL-alanine replaced with 10.5 mM D-mannitol) had no effect on V_t of either middle or posterior midgut epithelia. After bilateral K^+ removal, V_t changed from −26.9 ± 3.8 mV to −22.2 ± 2.9 mV ($n = 9$, $p > 0.06$) in the middle midgut and from −50.4 ± 8.1 mV to −49.4 ± 8.7 mV ($n = 3$, $p > 0.2$) in the posterior midgut respectively. Similarly, bilateral removal of K^+ did not change the R_t and I_{sc}. R_t changed from 933 ± 277 Ω • cm^2 to 805 ± 214 Ω • cm^2 ($n = 9$, $p > 0.2$) in the middle midgut and from 978 ± 199 Ω • cm^2 to 1000 ± 162 Ω • cm^2 ($n = 3$, $p > 0.8$) in the posterior midgut. Calculated short-circuit current (I_{sc}), in middle midgut changed from 43.3 ± 8.8 μA • cm^{-2} to 37.4 ± 7.4 μA • cm^{-2} ($n = 9$; $p > 0.06$); in the posterior midgut I_{sc} changed from 54.8 ± 9.8 μA • cm^{-2} to 49.8 ± 5.0 μA • cm^{-2} ($n = 3$; $p > 0.05$). In the posterior midgut, amiloride, bumetanide and ouabain (all at 10^{-4} M concentration), applied bilaterally, had no effect on V_t.

Figure 7 shows the effects of 3.5 μM Bafilomycin-A_1 in the bath on V_t, V_a and V_b. Bafilomycin-A_1 depolarized V_t and V_b, and to a smaller extent V_a (Fig. 7A). These effects were qualitatively similar but more pronounced in the posterior midgut (Fig. 7*B*). These effects were irreversible and the highest concentrations that could be applied was 7 μM of Bafilomycin-A_1, which caused ≈ 60% inhibition of V_t Smaller doses of Bafilomycin-A_1 produced qualitatively similar depolarization that was reversible. Luminal Bafilomycin-A_1 (≈ 1 μM), applied to the posterior midgut only, was without any effect.

Bafilomycin-A_1 (3.5 to 5.0 μM) depolarized V_t from −34.5 ± 2.7 mV to −23.7 ± 2.4 mV ($n = 5$;

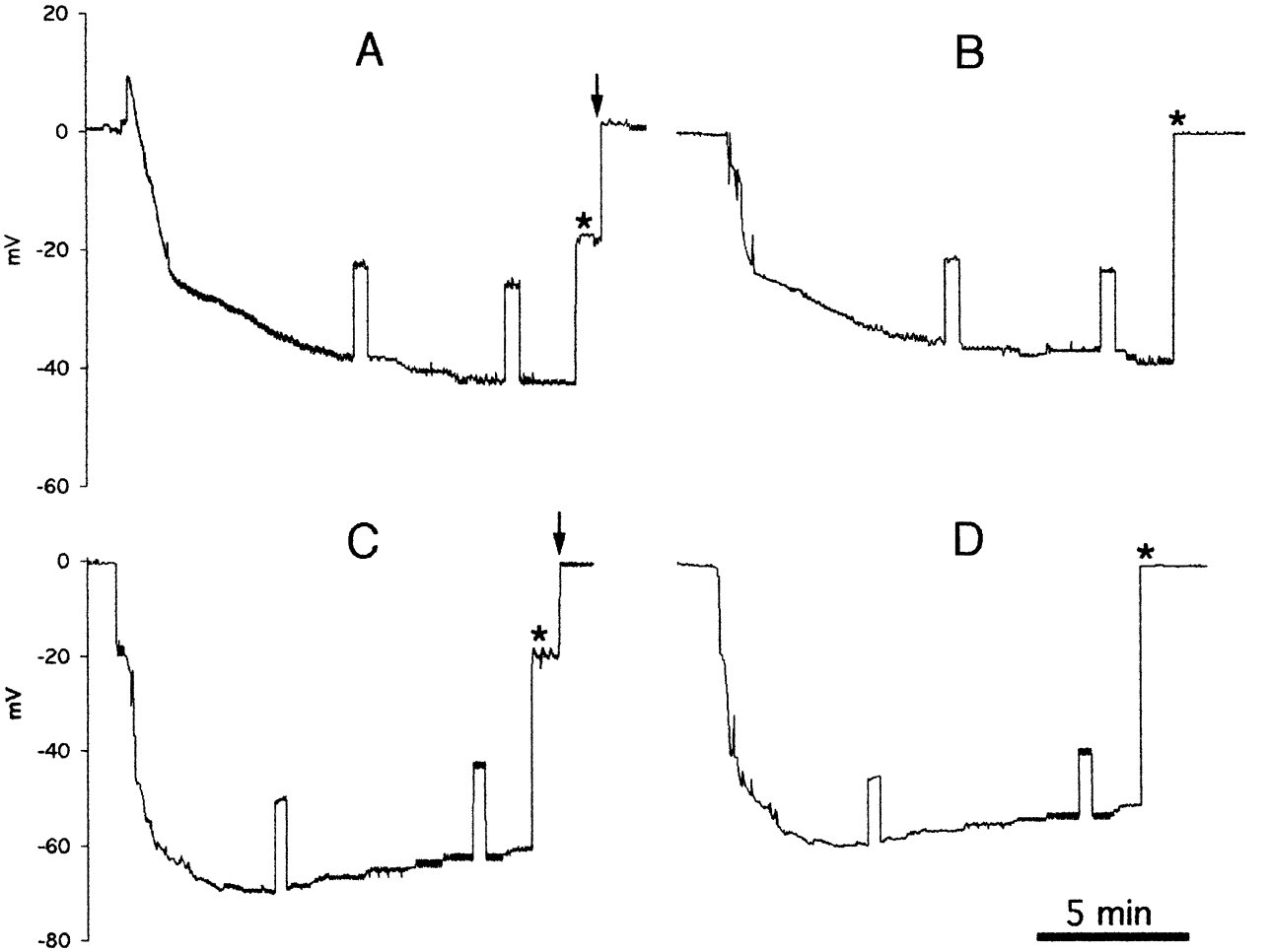

Fig. 4. Midgut transepithelial potential (V_t). (*A*) and (*B*) Middle midgut potential from perfusion (*A*) and collection (*B*) pipette. (*C*) and (*D*) Posterior midgut potential from perfusion (*C*) and collection (*D*) pipette. Current pulses (≈100 nA) cause displacements of V_t for transepithelial resistance (R_t) measurement. Release of midgut from the collection pipette (∗) attenuates V_t at the perfusion end and release of perfusion end (*arrows*) restores all pipette potentials to zero.

$p < 0.001$) and increased R_t from 657 ± 67 Ω • cm^2 to 859 ± 66 Ω • cm^2 ($n = 5$, $p < 0.001$) in the middle midgut. Likewise, it depolarized V_t from −43.3 ± 2.8 mV to −26.1 ± 1.9 mV ($n = 16$; $p < 0.001$) and increased R_t from 1010 ± 98 Ω • cm^2 to 1349 ± 98 Ω • cm^2 ($n = 16$, $p < 0.001$) in the posterior midgut segments. Bafilomycin-A_1 decreased I_{sc} in the middle midgut from 55 ± 6.6 μA • cm^{-2} to 29 ± 4.8 μA • cm^{-2} ($n = 5$; $p < 0.001$); likewise, I_{sc} in the posterior midgut segment decreased from 49 ± 4.8 μA • cm^{-2} to 20 ± 1.3 μA • cm^{-2} ($n = 16$; $p < 0.001$).

As the above data provided strong evidence for the presence of a basal H$^+$-V-ATPase we sought to establish whether significant H$^+$ accumulation could take place in the confined basal extracellular labyrinth (BEL) as a consequence of H$^+$ pumping. Figure 8 shows the advancement of a pH electrode in steps of 4 μm with high-precision piezo stepping after impalement of an adjacent cell with a membrane potential electrode (V_b). The advancement of a pH electrode (Fig. 8*a–g*) showed clear stepwise decrease in the extracellular pH (a pH- selective liquid ion exchanger microelectrode detects positive potentials with decreasing pH). Figure 8*g* shows impalement and crossing of the basal membrane by the pH electrode and results in the negative voltage step. The extracellular pH values in the radially inward direction beginning at the basement membrane plane are shown in the ordinate at right.

The intracellular pH (pH_i) was measured using simultaneous impalement of nearby cells with a membrane potential microelectrode and a pH microelectrode. The cells in the middle midgut segment had a mean pH_i of 7.11 ± 0.16 ($n = 10$) and the posterior midgut cells had a pH_i of 7.36 ± 0.01 ($n = 12$). Bafilomycin-A_1 (3–5 μM) applied to the bath, acidified pH_i from 6.98 ± 0.2 to 6.68 ± 0.15 ($n = 6$). In both middle and posterior midgut preparations the pH very close to the basement membrane

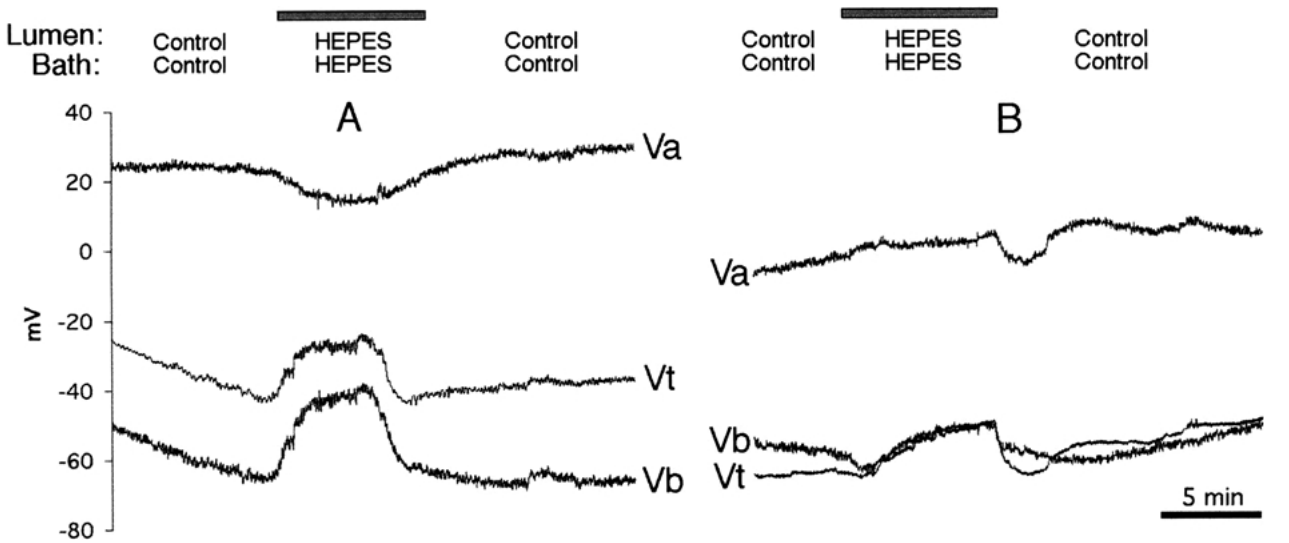

Fig. 5. Effect of HCO_3^- removal. (*A*) Middle midgut. (*B*) Posterior midgut. V_a, apical membrane potential; V_t, transepithelial potential; V_b, basal membrane potential. Bilateral substitution of HCO_3^- (*Control*) with HEPES (Table 1, *Solution a* replaced with *Solution b* on both sides) reversibly depolarizes V_t. Notice that V_b depolarizes much more than V_a.

or possibly in the BEL was 4.78 ± 0.01 (n = 13) for middle midgut cells and 4.34 ± 0.14 (n = 16) for posterior midgut cells.

Discussion

This study demonstrates the feasibility of isolating heterogeneous regions of larval *Drosophila* midgut epithelium and perfusing homogeneous segments to achieve full control of solution composition, voltage and pressure on both sides of the epithelium while retaining viability for substantial periods of time in vitro (up to 2 hours). The single layer of a small number of cells, reasonable homogeneity of cell type, few barriers in series with the epithelium, and short path lengths (< 2 μm) to the bulk phase (either lumen or bath) makes it a particularly appealing preparation to study and model. We report the first stereological ultrastructural measurement under these conditions and correlate ultrastructural observations with overall electrical and transport properties.

Ultrastructural Correlates of Function

One of the striking results of this preparation is the length of the junctional complex between cells and the almost complete absence of any lateral intercellular space (LIS). This is in contrast to other mammalian tight epithelia where an LIS is still found. This poses the technical challenge of short-circuiting of the epithelium if it is imperfectly sealed at both ends, unlike leaky epithelia like the proximal renal tubule, where a single-ended perfusion of a tubule can still give a reliable transepithelial potential (V_t) measurement (Tripathi et al., 1987). We have shown (Fig. 4) that it is possible to have adequate electrical sealing of this preparation with cannulation of both ends, and the small attenuation of potential during current injection indicates that it is possible to have good and uniform voltage control despite the constraints of tubular geometry. The long LIS also predicts effective intercellular adhesion even in the face of adverse hydrostatic pressure gradients.

Fig. 9 shows an equivalent electrical circuit of the two cell membranes in parallel with the lateral intercellular junction. The sum of V_a and V_b is V_t, which also is seen across the junction. Maneuvers that produce changes in membrane potentials usually show a larger effect on the basal membrane (Fig. 5*A*). This correlates with the fact that the amplifications of apical and basal membranes are 17- versus 7- fold respectively, predicting a larger conductance for the apical membrane.

Tests designed to inhibit transport (removal of Na^+, HCO_3^- or Cl^-) produced changes in V_a, V_b, V_t, R_t and I_{sc} (Figs. 5 and 6; Table 2, columns 3 – 5) that indicate significant conductive permeation through either one or both membranes. Morphometry showed that unilateral and bilateral removal of Na^+ caused progressive loss of surface membrane and internalization of these membranes into vacuoles, leading to a substantial reduction in the surface-to-volume ratios of the cells. The inhibitions of transport can mainly be ascribed to these dimensional changes. Bilateral removal of Na^+ has the extreme consequence of complete ablation of the BEL. Clearly these ion substitutions have deleterious effects that are only partly revealed by electrophysiology. The reasons for membrane internalization are not clear. Removal of

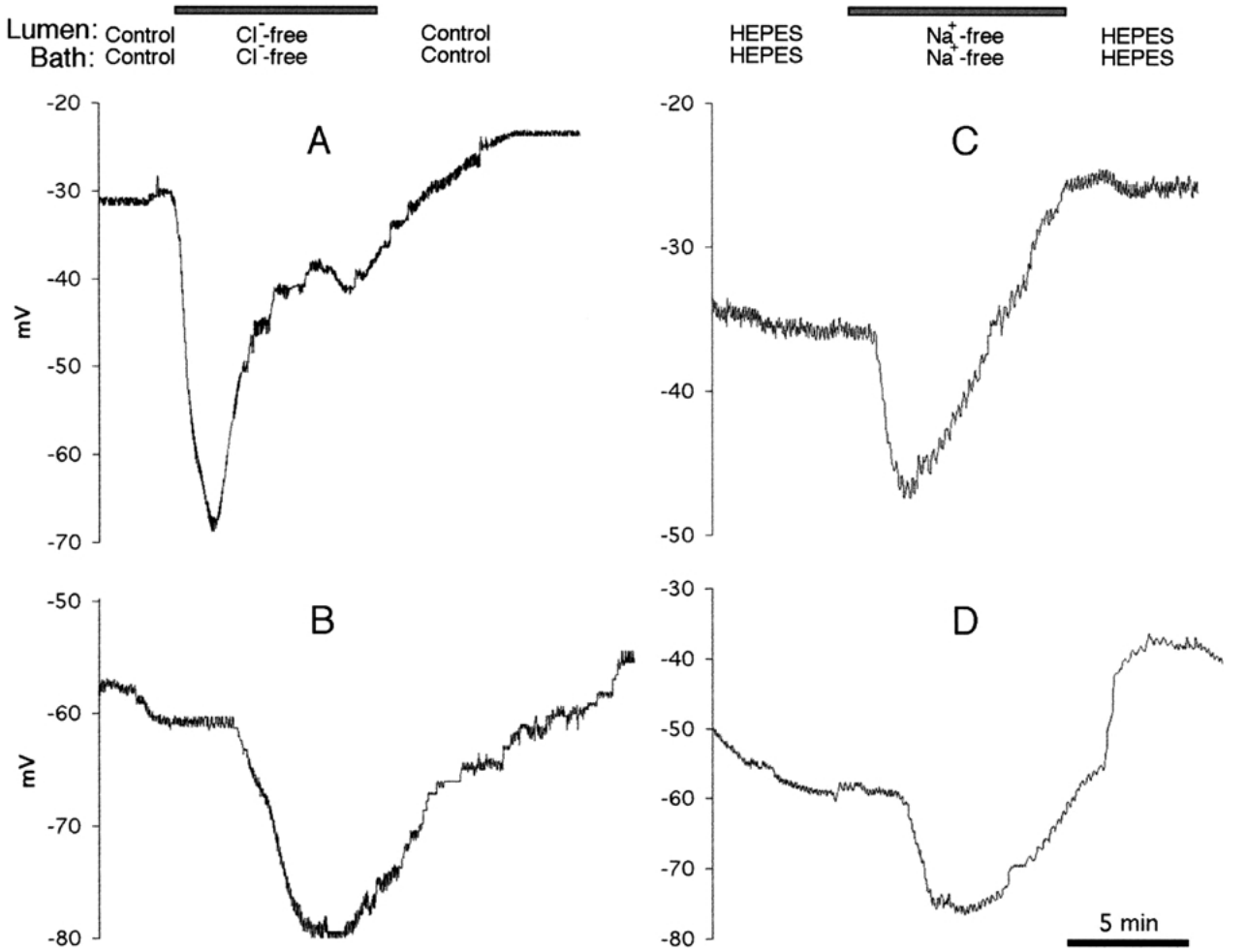

Fig. 6. (*A*) and (*B*) Effect of Cl^- removal. Perfusion end V_t is shown for (*A*) middle and (*B*) posterior midgut. Simultaneous bilateral removal of Cl^- (Solution a replaced with Solution c on both sides) cause variable transient changes in V_t that are reversible, accompanied by large increase in R_t. Bilateral restoration of Cl^- with Solution a reverses this effect. (*C*) and (*D*) Effect of Na^+ removal. (*C*) Middle midgut, (*D*) posterior midgut. Simultaneous bilateral removal of Na^+ (Solution a replaced with Solution d on both sides) causes variable transient changes in V_t that are partly reversible.

HCO_3^- had little effect on R_t and the depolarization of the cell could reflect possible electrogenic coupling with another solute, possibly Na^+. Removal of Cl^- produced a major decrease in conductance and I_{sc}. This indicates a high background anion conductance of the membranes, with possible coupling to other solutes. The substantial rise in R_t is not consistent with neutral exchange of HCO_3^- for Cl^- proposed in other midgut epithelia (Boudko et al., 2001b).

Electrogenic H^+ Transport

Figure 9 shows that currents generated by either apical or basal membrane circulate through the junctional complex. Depolarization of V_t and V_b is seen only when Bafilomycin-A_1 is applied from the bath. This is most likely due to an inhibition of a V-H$^+$-ATPase transferring positive charge outwards through the basal membrane. The higher V_t in the posterior midgut, as compared to the middle midgut, is compatible with a higher rate of electrogenic H^+ extrusion to the basal side in the former. The higher control intracellular pH_i measured by pH-selective microelectrodes and the higher alkalinization of the lumen (Fig. 1) in the posterior segment support this hypothesis, as does the fall in pH_i after inhibition of the V-H$^+$-ATPase. The accumulation of H^+ in the unstirred layers next to the basal membrane reported here (Fig. 8) is similar to that detected in mosquito larvae (Boudko et al., 2001a). The mechanism of increase in R_t seen with Bafilomycin-A_1 is not obvious, and could be related to the inactivation of channels gated directly or indirectly by H^+. Our observation of the basal (but not apical) effect of Bafilomycin-A_1 is similar to those of Beyenbach, Pannabecker and Nagel (2000). However, H^+ flux in *A. aegypti* reported by Beyenbach et al. (2000) is in a secretory direction and the V-H$^+$-ATPase is thought to be located apically in *A. aegypti*. The molecule species carrying base into the lumen is not clear, but could

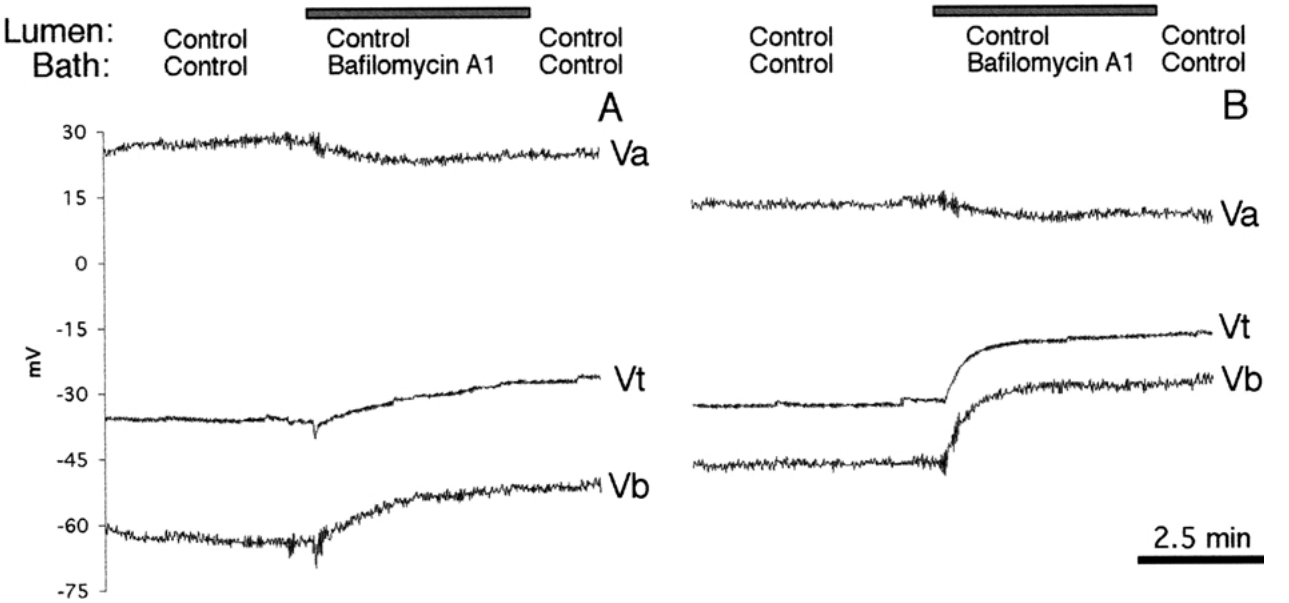

Fig. 7. Effect of basal Bafilomycin-A_1. (*A*) Middle midgut, (*B*) posterior midgut. V_a, apical membrane potential; V_t, transepithelial potential; V_b, basal membrane potential. Following a period of control perfusion with Solution a on both sides, 3.5 μM Bafilomycin-A_1 superfused in the bath depolarizes V_t, V_b, and V_a, V_b depolarizes much more than V_a.

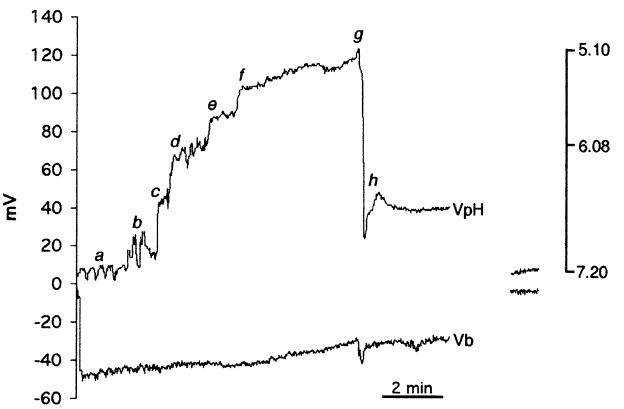

Fig. 8. pH gradients in the basal labyrinth. Left ordinate is potential of microelectrodes. Upper trace V_{pH} shows the absolute potential of a pH-selective microelectrode. Lower trace is the basal potential recorded by an intracellular microelectrode V_b. As the pH microelectrode is advanced radially inward into the gut wall by a piezo-stepper in steps of 4 μm, there is an increasing positive signal from the pH microelectrode. The extracellular pH is indicated by the ordinate on the right. High-speed impalement of a cell results in the negative voltage step. Post-impalement control voltages are shown at right for each microelectrode.

well be HCO_3^-, driven by V_a and / or a symporter on the apical membrane. A basal localization of V-ATPase is well known in type B cells of rat kidney (Brown et al., 1992) and mosquito midgut (Zhuang et al., 1999; Boudko et al., 2001b). Further experiments using fluorescence measurements of pH gradients, combined with an electrophysiological approach, are clearly required to obtain a complete description of the barriers and mechanisms of H^+ transport.

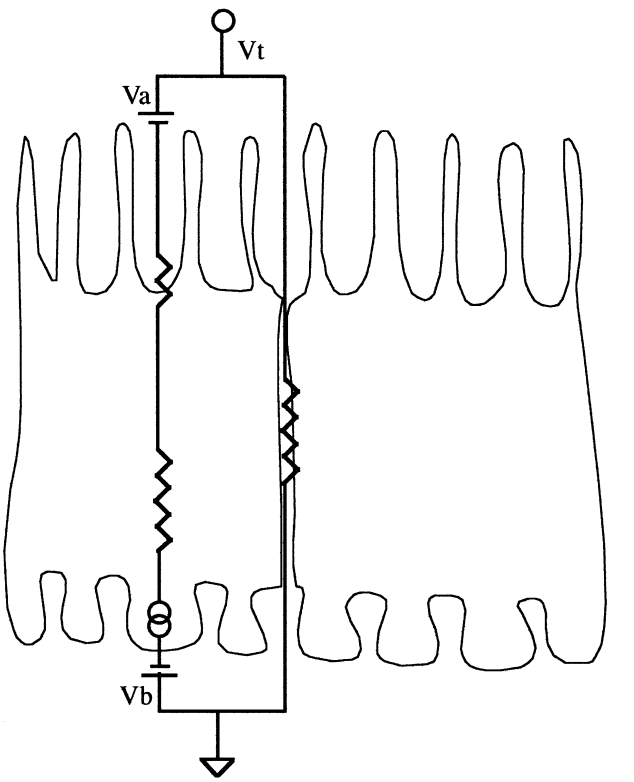

Fig. 9. Equivalent circuit of middle and posterior midgut epithelium. The high transepithelial resistance is due primarily to extremely long intercellular junctions and basal cell membrane resistance. The basal membrane is more resistive than the apical membrane. The electrogenic V-H$^+$-ATPase is modeled as a constant current source that transfers positive charge (H^+) to the basal side. V_t measured across the entire epithelium is the sum of V_a and V_b.

We record our gratitude to the late Peter D'Souza and to J. N. Parmar for fabrication of the microperfusion apparatus and excellent machining support. We thank T. V. Abraham for electronics and data acquisition software. Supported by Interdisciplinary Programme 10P-809.

References

Ashburner, M. 1989. *Drosophila*. A Laboratory Manual. Second edition. Cold Spring Harbor Laboratory Press, New York

Berenbaum, M. 1980. Adaptive significance of midgut pH in larval *Lepidoptera*. *Am. Nat.* **115:**138–146

Beyenbach, K.W., Pannabecker, T.L., Nagel, W. 2000. Central role of the apical membrane H^+-ATPase in electrogenesis and epithelial transport in malpighian tubules. *J. Exp. Biol.* **203:**1459–1468

Boudko, D.Y., Moroz, L.L., Harvey, W.R., Linser, P.J. 2001a. Alkalinization by chloride / bicarbonate pathway in larval mosquito midgut. *Proc. Natl. Acad. Sci. USA* **98:**15354–15359

Boudko, D.Y., Moroz, L.L., Linser, P.J., Trimarchi, J.R., Smith, P.J., Harvey, W.R. 2001b. *In situ* analysis of pH gradients in mosquito larvae using non-invasive, self-referencing, pH-sensitive microelectrodes. *J. Exp. Biol.* **204:**691–699

Brown, D., Gluck, S., Hartwig, J. 1987. Structure of the novel membrane-coating material in proton-secreting epithelial cells and identification as an H^+ATPase. *J. Cell Biol.* **105:**1637–1648

Dadd, R.H. 1975. Alkalinity within the midgut of mosquito larvae with alkaline-active digestive enzymes. *J. Insect Physiol.* **21:**1847–1853

Dow, J.A.T. 1984. Extremely high pH in biological systems; a model for carbonate transport. *Am. J. Physiol.* **246:**R633–R635

Dow, J.A.T. 1986. Insect midgut function. *Adv. Insect Physiol.* **19:**187–328

Dow, J.A.T. 1992. pH gradients in Lepidopteran midgut. *J. Exp. Biol.* **172:**355–375

Dubreuil, R.R., Frankel, J., Wang, P., Howrylak, J., Kappil, M., Grushko, T.A. 1998. Mutations of α Spectrin and labial block cuprophilic cell differentiation and acid secretion in the middle midgut of *Drosophila* larvae. *Dev. Biol.* **194:**1–11

Dubreuil, R.R., Grushko, T., Baumann, O. 2001. Differential effects of a labial mutation on the development, structure, and function of stomach acid-secreting cells in *Drosophila melanogaster* larvae and adults. *Cell Tissue Res.* **306:**167–178

Filippova, M., Ross, L.S., Gill, S.S. 1998. Cloning of the V ATPase B subunit cDNA from *Culex quinquefasciatus* and expression of the B and C subunits in mosquitoes. *Insect Mol. Biol.* **7:**223–232

Greenberg, B. 1968. Micro-potentiometric pH determinations of muscoid maggot digestive tracts. *Ann. Entomol. Soc. Am.* **61:**365–367

Harrison, J.F. 2001. Insect acid-base physiology. *Annu. Rev. Entomol.* **46:**221–250

Klein U., Koch A., Moffett D.F. 1996. Ion transport in Lepidoptera. In: M.J. Lehane P.F. Billingsley, editors. Biology of the Insect Midgut. Chapman & Hall, London, pp. 236–264

Martin, J.S., Martin, M.M. 1984. Surfactants: their role in preventing the precipitation of proteins by tannins in insect guts. *Oecologia* **61:**342–345

Maunsbach, A.B., Boulpaep, E.L. 1984. Quantitative ultrastructure and functional correlates in proximal tubule of *Ambystoma* and *Necturus*. *Am. J. Physiol.* **246:**F710–F724

Schultz, J.C., Lechowicz, M.J. 1986. Host plant, larval age and feeding behavior influence midgut pH in the gypsy moth (*Lymantria dispar*).. *Oecologia* **71:**133–137

Shanbhag, S.R., Singh, K., Singh, R.N. 1992. Ultrastucture of the femoral chordotonal organs and their novel synaptic organization in the legs of *Drosophila melanogaster* Meigen (Diptera: Drosophilidae). *Int. J. Insect Morphol. & Embryol* **21:**311–322

Shanbhag, S., Tripathi, S. 2005. An electrogenic V-H^+-ATPase drives electrolyte transport in the isolated perfused larval *Drosophila* midgut. *J. Physiol.* **565P:**C3

Terra W.R., Ferriera C., Baker J.E. 1996. Compartmentalization of digestion. In: M.J. Lehane P.F. Billingsley, editors, Biology of the Insect Midgut. Chapman and Hall, London, pp. 226–235

Tripathi, S., Morgunov, N., Boulpaep, E.L. 1985. Submicron tip breakage and silanization control improve ion-selective microelectrodes. *Am. J. Physiol.* **249:**C514–C521

Tripathi, S., Boulpaep, E.L., Maunsbach, A.B. 1987. Isolated perfused *Ambystoma* proximal tubule: hydrodynamics modulates ultrastructure. *Am. J. Physiol.* **252:**F1129–F1147

Tripathi, S., Boulpaep, E.L. 1988. Cell membrane water permeabilities and streaming currents in *Ambystoma* proximal tubule. *Am. J. Physiol.* **255:**F188–F203

Wagner, C.A., Finberg, K.E., Breton, S., Marshansky, V., Brown, D., Geibel, J.P. 2004. Renal Vacuolar H^+-ATPase. *Am. J. Physiol* **84:**1263–1314

Zhuang, Z., Linser, P.J., Harvey, W.R. 1999. Antibody to H^+V-ATPase subunit E colocalizes with portasomes in alkaline larval midgut of a freshwater mosquito (*Aedes aegypti* L.). *J. Exp. Biol.* **202:**2449–2460